Journal of Non-Newtonian Fluid Mechanics 284 (2020) 104376

Contents lists available at ScienceDirect

Journal of Non-Newtonian Fluid Mechanics

journal homepage: www.elsevier.com/locate/jnnfm

Particle migration in channel flow of an elastoviscoplastic fluid

Emad Chaparian [*,1], Mehdi N. Ardekani, Luca Brandt, Outi Tammisola

Linné FLOW Centre and SeRC, Department of Engineering Mechanics, Royal Institute of Technology (KTH), SE-100 44, Stockholm, Sweden

ARTICLE INFO

Keywords:
Yield-stress fluid
Elastoviscoplastic fluid
Viscoelastic fluid
Particle migration

ABSTRACT

We study the dynamics of a neutrally buoyant rigid sphere carried by an elastoviscoplastic fluid in a pressure-driven channel flow numerically. The yielding to flow is marked by the *yield stress* which splits the flow into two main regions: the core unyielded region and two sheared yielded regions close to the walls. The particles which are initially in the plug region are observed to translate with the same velocity as the plug without any rotation/migration. Keeping the Reynolds number fixed, we study the effect of elasticity (Weissenberg number) and plasticity (Bingham number) of the fluid on the particle migration inside the sheared regions. In the viscoelastic limit, in the range of studied parameters (low elasticity), inertia is dominant and the particle finds its equilibrium position between the centreline and the wall. The same happens in the viscoplastic limit, yet the yield surface plays the role of centreline. However, the combination of elasticity and plasticity of the suspending fluid (elastoviscoplasticity) trigger particle-focusing: in the elastoviscoplastic flow, for a certain range of Weissenberg numbers (≈ 0.5), isolated particles migrate all the way to the centreline by entering into the core plug region. This behaviour suggests a particle-focusing process for inertial regimes which was not previously found in a viscoelastic or viscoplastic carrying fluid.

1. Introduction

Transporting suspension of particles in a yield-stress fluid is a crucial problem to be understood due to intrinsic complexities from the carrying fluid rheology to the particle dynamics. A short list of applications may include, but is not limited to, construction (e.g. pumping concrete [1]) and oil & gas industries (e.g. fracturing flows [2]). Efforts of Segré & Silberberg [3–5] and other scholars uncovered the behaviour of particles suspended in a Newtonian fluid Poiseuille flow: from theoretical frameworks [6–8] that extensively revealed features of this problem at the low Reynolds number limit, to experimental validations/extensions [9]. Further studies uncovered the features of the problem in non-cylindrical conduits [10] and migration of deformable and non-spherical particles [11–13].

The Poiseuille flow of a yield-stress fluid is split into two main regions: the sheared yielded region(s) close to the wall(s) and the unyielded core. The particle dynamics in each region has its own complexity: in the yielded regions, it comes from different sources such as the non-linearity of the fluid behaviour and particle–particle & particle–wall collisions, whereas in the core unyielded region particles might be trapped [14–16] because of the small stresses compared to the yield stress. In the present study, we will shed light on the particle migration inside the sheared yielded regions. Regarding applications, the subject of this work is relevant to particle sorting/separation and manipulation of cells in microfluidic devices [17], fractionation using yield-stress fluids [18], and the homogeneity during pumping a suspension [19,20].

To this aim, the fluid rheology is represented by a sophisticated model – elastoviscoplasticity [21] – to capture more realistic aspects of the problem beyond the 'simple' yield-stress models. The existing literature concerning the particle migration within the viscoelastic and viscoplastic fluid flows is quickly reviewed in what follows.

1.1. Particle migration in poiseuille flow of a viscoelastic fluid

In contrast to a Newtonian Stokes flow (when the inertia is completely neglected from the equations of motion) where a single particle does not migrate in a unidirectional flow [6,22], a particle in an inertialess viscoelastic Poiseuille flow migrate either towards the centre or the walls based on many factors such as its initial position and shear-thinning effects [23–25]. Inertia promotes particle migration as well but in a different way: it pushes the particles towards an equilibrium position in the middle of the channel half width, whereas the elasticity of the fluid causes lateral motion towards the centreline or walls. Hence, in the inertial Poiseuille flow of a viscoelastic fluid, the balance between these two competing effects results in different equilibrium positions depending on the Reynolds number and Weissenberg number

* Corresponding author.
E-mail address: emad@math.ubc.ca (E. Chaparian).
[1] Present address: Mathematics Department, University of British Columbia, Vancouver, BC, V6T 1Z2, Canada.

https://doi.org/10.1016/j.jnnfm.2020.104376
Received 24 April 2020; Received in revised form 24 July 2020; Accepted 13 August 2020
Available online 22 August 2020

(ratio of the fluid's relaxation time to the flow's time scale). This analysis is not trivial: as measured by Di Carlo et al. [26], the lateral force on the particle in a viscous inertial flow collapses on 'master curves' (close to the wall and in the vicinity of the channel centreline with different scalings), but when the fluid elasticity emerges then the lateral force distribution is markedly complicated [27]. Even multiple stable and unstable particle final positions may occur which is mostly attributed to the combined effects of shear-thinning and elasticity of the fluid. Hence, the final position does not only depend on the Reynolds number and the Weissenberg number, but it also depends on the initial position of the particles [28]. The complexity of the problem dramatically increases in 3D background flows as discussed in [29].

1.2. Particle migration and stability in yield-stress fluid poiseuille flow

Particle migration within a Poiseuille flow of a yield-stress fluid and the entrapment of particles inside the core unyielded plug are less understood. Very recently, Siqueira & de Souza Mendes [30] studied the particle migration in an 'apparent' yield-stress fluid by coupling the regularised effective viscosity of a viscoplastic material with closures for the suspension viscosity and shear-induced particle migration. These authors report high particle concentration in the plug region at shorter time scales, however, due to the closures used, eventually (at larger time scales) the plug zone is totally depleted from the particles. However, using the direct numerical simulation of the unregularised rheology, Chaparian & Tammisola [16] demonstrated that neutrally buoyant particles are strictly *stable* (i.e. move with the same velocity as the plug without any rotation or migration) in the core unyielded plug. Moreover, Chaparian & Tammisola [16] found that the core unyielded plug can grow locally, under some circumstances, to enclose/stabilise adjacent particles. This picture holds even for non-neutrally buoyant particles, although, they lose their stability with smaller buoyancy than sedimentation within a bath of quiescent yield-stress fluid [31–33]. Some of these features have been observed in the experiments by Merkak et al. [14,15] in inertialess viscoplastic pipe flows (maximum particle Reynolds number $\sim O(10^{-1})$). The main observations of Merkak et al. [14,15] for neutrally buoyant particles are highlighted below:

(i) Particles situated completely or partly in the sheared zones (yielded zones) translate and rotate with velocities that are functions of the yield stress and the pressure drop (i.e. the Bingham number). For small particles, migration towards the centre of the pipe was recorded, while no penetration into the plug zone was observed. This was sensitive to the initial position of the particles in the sheared zones since the particles which are initially close to the wall did not migrate.

(ii) Large particles which are extremely close to or in contact with the pipe wall adhere to the wall and do not move.

Some of the observations in [30] (e.g. particle depletion from the plug) and [14,15] (e.g. particle stock at the walls) appear counterintuitive. This fact signals the need of further studies on this problem by direct numerical simulations of unregularised rheology, which is the approach of the present study. In addition, we quantify the equilibrium position of the particles, address the inertial viscoelastic and viscoplastic limits of the problem and also interesting intermediate elastoviscoplastic regime. Indeed, we study the effect of elasticity of the yield-stress fluid (elastoviscoplastic regime) on the particle migration.

The outline of the paper is as follows. In Section 2, we set out the studied problem and quickly review the features of the implemented numerical method. The main results are presented in Section 3 and conclusions drawn in Section 4.

2. Problem statement

We consider the motion of a rigid neutrally-buoyant spherical particle of diameter $\hat{D}$ in the inertial elastoviscoplastic fluid flow between two infinite parallel plates separated by the gap $\hat{H}$; see Fig. 1. The wall-normal position of the centre of the particle is denoted by $\hat{y}^p$. The x-axis is aligned with the axial centreline of the channel. In the entire paper, the 'hat' sign ($\hat{\cdot}$) indicates dimensional quantities.

2.1. Scalings and remarks

The important non-dimensional parameters defining our problem are: Bingham number, Weissenberg number, Reynolds number, and the blockage ratio,

$$B = \frac{\hat{\tau}_Y \hat{D}}{\hat{\mu}\,\hat{U}}, \quad Wi = \frac{\hat{\lambda}\,\hat{U}}{\hat{D}}, \quad Re = \frac{\hat{\rho}\,\hat{U}\hat{D}}{\hat{\mu}}, \text{ and } \xi = \frac{\hat{H}}{\hat{D}}.$$

The blockage ratio represents the ratio of the channel width to the particle diameter. Here, $\hat{\tau}_Y$ is the yield stress and $\hat{\lambda}$ the relaxation time of the fluid. The mean velocity of the flow is designated by $\hat{U}$ and the total viscosity of the fluid ('solvent viscosity' + 'plastic viscosity' $= \hat{\mu}_1 + \hat{\mu}_2$) by $\hat{\mu}$ [34]. Upon scaling the velocity vector ($\hat{\boldsymbol{u}}$) with the bulk velocity of the flow ($\hat{U}$), $\hat{p}$ with $\hat{\rho}\hat{U}^2$, and the extra stress tensor ($\boldsymbol{\tau}$) with the characteristic viscous stress ($\hat{\mu}\hat{U}/\hat{D}$), we find the dimensionless governing and constitutive [21] equations as,

$$\frac{D\boldsymbol{u}}{Dt} = -\boldsymbol{\nabla} p + \frac{1}{Re}\left(\boldsymbol{\nabla}\cdot\boldsymbol{\tau} + \beta\,\boldsymbol{\nabla}\cdot\dot{\boldsymbol{\gamma}}\right) + \boldsymbol{f}, \tag{1}$$

$$Wi\,\overset{\triangledown}{\boldsymbol{\tau}} + \left(1 - \frac{B}{\|\boldsymbol{\tau}\|_{\mathrm{v}}}\right)_{+}\boldsymbol{\tau} = (1-\beta)\dot{\boldsymbol{\gamma}}, \tag{2}$$

respectively, where $\overset{\triangledown}{\boldsymbol{\tau}}$ is the upper-convected derivative, $\|\boldsymbol{\tau}\|_{\mathrm{v}}$ the *equivalent von Mises stress*, $\beta = \hat{\mu}_1/\hat{\mu}$ the viscosity ratio, $\dot{\boldsymbol{\gamma}}$ the rate of strain tensor, and $(g)_+$ denotes the positive part of g. The presence of the particle is modelled with the external force $\boldsymbol{f}$ (i.e. immersed boundary force); details are given in Section 2.2.

It should be mentioned that other physical scalings are possible as well especially by considering the effective viscosity (see [35]). We will come back to this point later in Section 4.

Please note that generally for an elastoviscoplastic fluid, $\boldsymbol{\tau}$ is not deviatoric and p is only a Lagrangian multiplier enforcing the incompressibility constraint ($\boldsymbol{\nabla}\cdot\boldsymbol{u} = 0$). The pressure gradient in the flow direction (x-direction) is included in p to enforce a constant bulk velocity $\hat{U}$. The Cauchy stress for the elastoviscoplastic fluid is defined as $\boldsymbol{\sigma} = -p\mathbf{1} + \boldsymbol{\tau} + \beta\dot{\boldsymbol{\gamma}}$.

The rheological model used is capable of representing both the viscoelastic (Oldroyd-B fluid; $B = 0$) and viscoplastic (Bingham fluid; $Wi = 0$) limits of the problem. Please note that shear-thinning effects are not included in this model to limit the already large number of governing parameters, yet capturing novel interesting features. In other words, the Oldroyd-B and the Bingham models which are combined to form this elastoviscoplastic model are not individually "shear-thinning" models.

Particle motion satisfies Euler–Newton equation:

$$Re\; V_p \frac{\mathrm{d}\boldsymbol{u}_p}{\mathrm{d}t} = \int_{\partial\mathbb{P}} \boldsymbol{\sigma}\cdot\boldsymbol{n}\;\mathrm{d}A, \tag{3a}$$

$$Re\; V_p \boldsymbol{I}_p \frac{\mathrm{d}\boldsymbol{\Omega}_p}{\mathrm{d}t} = \int_{\partial\mathbb{P}} \boldsymbol{r}\times(\boldsymbol{\sigma}\cdot\boldsymbol{n})\;\mathrm{d}A, \tag{3b}$$

$$\boldsymbol{u} = \boldsymbol{u}_p + \boldsymbol{r}\times\boldsymbol{\Omega}_p \quad \text{on } \partial\mathbb{P}, \tag{3c}$$

where $\mathbb{P}$ represents the particle domain. Dimensionless volume, moment of inertia, linear velocity, and rotation velocity of the particle are denoted by V_p, $\boldsymbol{I}_p$, $\boldsymbol{u}_p$, and $\boldsymbol{\Omega}_p$, with the particle diameter $\hat{D}$ as the length scale. Please note that the Reynolds number here is defined based on the particle diameter. The Reynolds number based on the

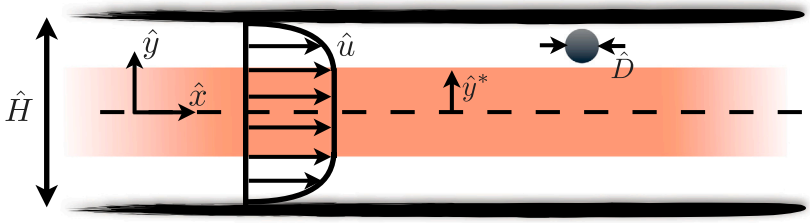

Fig. 1. Schematic of the problem. The x-axis is aligned with the centreline of the channel that is formed by the two infinite parallel plates separated by the gap $\hat{H}$. A rigid neutrally-buoyant spherical particle of diameter $\hat{D}$ is carried by the elastoviscoplastic fluid Poiseuille flow. The position of the yield surface in the absence of any particle (undisturbed flow) is denoted by $\hat{y}^*$; the core unyielded region is illustrated in red.

channel width which is more accepted in the particle-free (single phase) flows is equal to $Re\ \xi$.

In what follows, the position of the yield surface in the single-phase Poiseuille flow in the absence of any particle is represented by y^* (see Appendix) and the equilibrium position of the particle at the final stage is designated by y^e.

2.2. Numerical details

A detailed explanation of the numerical method used in the present study has been recently published by the authors [36]. To highlight, a 3D numerical solver is used that combines a highly scalable FFT-based pressure solver with the constitutive equation (2), allowing direct numerical simulations of viscoelastic and elastoviscoplastic complex flows such as turbulent flows [37] and flows in porous media [38]. The particle-fluid interactions are resolved using the discrete forcing Immersed Boundary Method (IBM) [39]. In this method, the carrier phase is solved on a fixed Eulerian grid, whereas the interface is represented by a set of Lagrangian points uniformly distributed on the particle surface. The additional term $\boldsymbol{f}$ on the right hand side of Eq. (1) is the IBM force field, active in the immediate vicinity of the particle surface to enforce the no-slip and no-penetration boundary conditions on $\partial\mathbb{P}$. Readers are refereed to [36] for the details/implementation.

The log-conformation method [40,41] is employed to overcome the well-known high Weissenberg number issue: numerical instabilities arising beyond a critical value of the Weissenberg number which makes it impossible to obtain discrete solutions; see [42]. Time marching is performed with a third-order explicit Runge–Kutta scheme except for the extra stress which is advanced with the Crank–Nicolson method. The spatial derivatives are approximated with second-order centred finite differences except for the advection term in the constitutive equation where the fifth-order WENO [43] is adopted.

The present method and its implementation have been extensively validated in our previous works, combining IBM with viscoelastic and elastoviscoplastic fluid solvers [36,44]. Regarding the simulations in the present work, we shall add that the resolution is chosen fine enough to ensure grid independency: the simulations are conducted on a uniform Cartesian grid with the resolution of 32 Eulerian grid points per particle diameter. The particle is represented by 3219 (dependent on the Eulerian resolution) Lagrangian points, uniformly distributed on its surface. The computational box has dimensions $15 \times 10 \times 5$ particle diameters in the streamwise (x), wall-normal (y) and spanwise (z) directions. Periodic boundary conditions are imposed in the x- (wall-parallel) and z-directions, while no-slip and no-penetration boundary conditions are applied at the top and bottom walls of the channel. It should be mentioned that the streamwise length of the numerical domain is chosen adequately large so that the flow and stress fields around the particle are not affected by the imposed periodicity.

3. Results and discussion

In this study, we focus on the individual and combined effects of elasticity and plasticity of the suspending fluid on the particle migration. Hence, we will vary the Weissenberg and Bingham numbers, while keeping the blockage ratio fixed at 10 and the Reynolds number at 20 in the entire study. To enable a direct comparison of the viscoelastic and viscoplastic limits of the problem, we also fix the viscosity ratio β at 0.5. This specific choice of β is a compromise, knowing that for most of the viscoelastic fluids β is large and on the other side, viscoplastic fluids have $\beta \to 0$. Chaparian et al. [38] have shown that the effect of β is small on the pressure driven flow of elastoviscoplastic fluids through a porous medium. Yet, the viscosity ratio may play a role in the present flow configuration, but its investigation is postponed to future studies.

In this section, we mostly discuss the cases in which the particles are initially in the sheared regions. Although not shown for the sake of brevity, particles which are initially in the core unyielded region translate with the same velocity as the plug without any migration/rotation. This has been previously demonstrated both numerically [16] and experimentally [14,15] for 'simple' viscoplastic suspending fluids.

The wall-normal position of the particles starting in the sheared regions are displayed in Fig. 2 where the horizontal axis shows time. All particles have been initiated in the bottom half of the channel. We vary the Bingham number between 0 and 0.4 and Wi between 0.1 and 1. As is clear from the cyan lines in Fig. 2(a), for the specified Reynolds and Weissenberg numbers, no particle focusing on the centreline or walls is observed in the viscoelastic flow. This means that inertia is dominant here, while for $Re \sim O(10^{-1})$ & $Wi \sim O(10)$, Villone et al. [25] observed that particles move towards either the centreline or walls based on their initial positions (i.e. elastic effects win over inertia).

Another interesting feature, in the viscoelastic flow within the range of studied parameters, is that the equilibrium position is a non-monotonic function of Wi: y^e is equal to 1.91 for $Wi = 0.1$ and increasing the Wi to 0.5 will push the equilibrium position slightly towards the centreline ($y^e \approx 1.5$), however, when $Wi = 1$, y^e moves away form the centreline ($y^e \approx 1.73$). This non-monotonic behaviour had been evidenced before by many scholars in the same context. For instance, very recently, Raffiee et al. [27] computed the force (elastic + inertial) acting on the particle as a function of Wi and the position of the particle. These authors demonstrated that in the inertial regime, at low Weissenberg numbers, the equilibrium position changes non-monotonically with Wi (see Fig. 3(b) of the mentioned reference) as a consequence of the complex interaction between wall effects, elastic and inertial forces. Moreover, Li et al. [29] studied the migration of particles hosted by a Giesekus fluid and observed that although increasing Wi initially forced the particles to go to the centre, increasing Wi further resulted in an equilibrium position in the middle of the duct width (see Fig. 3 of the mentioned reference: the dashed line-triangle, the dotted line-triangle, and the dashed–dotted line-full circle data).

In the present work, we show that this picture holds for the non-zero Bingham numbers (elastoviscoplastic fluid) as well. The red continuous line-squares in Fig. 2(a) show the case $Wi = 0.1$ & $B = 0.2$ in which

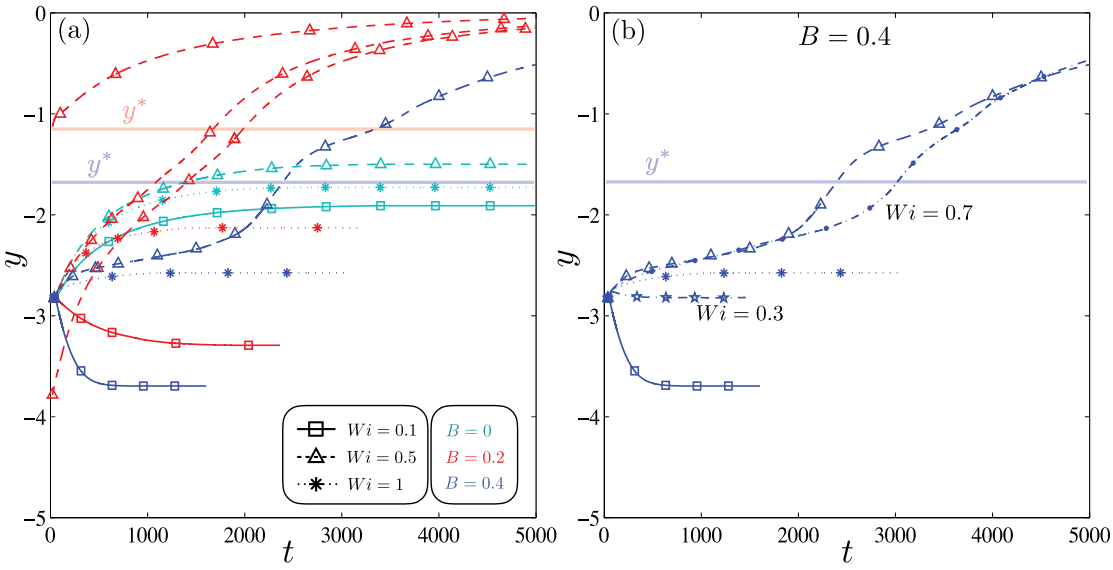

Fig. 2. Wall-normal position (y_p versus time) of the particles for different Weissenberg and Bingham numbers with different initial positions. The continuous lines with □ stand for $Wi = 0.1$, dashed lines with △ for $Wi = 0.5$, and dotted lines with ∗ for $Wi = 1$. Cyan colour represents the case $B = 0$, red the case $B = 0.2$, and blue the case $B = 0.4$. In the panel (b), only the data for the case $B = 0.4$ are shown for a better comparison: the symbols interpretations are the same as in the panel (a) and the dashed–dotted line-stars shows the case $Wi = 0.3$ and the dashed–dotted line-full circles the case $Wi = 0.7$. The position of the yield surfaces associated with the undisturbed Poiseuille flow (see Appendix) are marked with the continuous lines of light colour; the same as the corresponding Bingham number. In the range $0.1 \leqslant Wi \leqslant 1$, y^* does not change considerably and is mostly determined by the Bingham number. (For interpretation of the references to colour in this figure legend, the reader is referred to the web version of this article.)

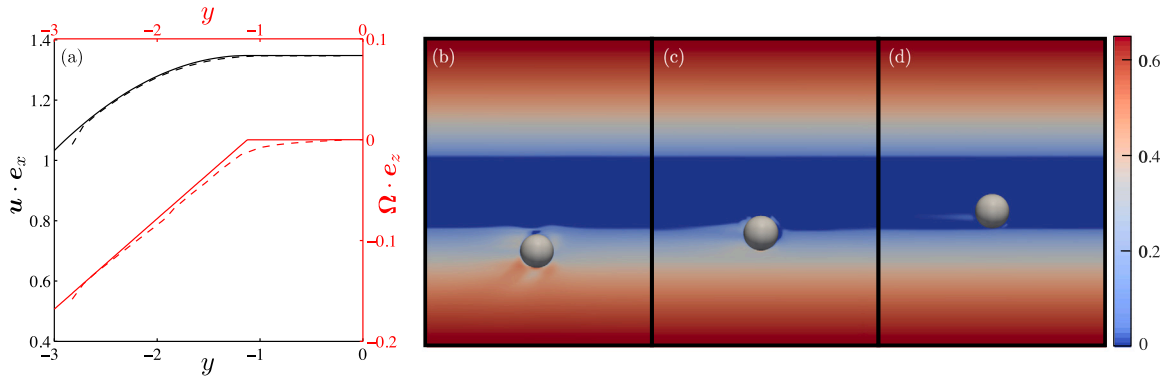

Fig. 3. Particle dynamics; case $Wi = 0.5$ & $B = 0.2$: (a) Velocity component in the axial direction (black colour) and rotation in the spanwise direction (red colour) versus the wall-normal position of the particle; the continuous lines correspond to the undisturbed flow (see Appendix) and the discontinuous lines represent the particle data extracted from the computations. Please note that the rotation of the undisturbed flow (the red continuous line), $\boldsymbol{\Omega} = \frac{1}{2}\boldsymbol{\nabla} \times \boldsymbol{u}$, which reduces to the local shear rate $(-\mathrm{d}u/\mathrm{d}y)$ since the undisturbed flow is unidirectional. Panels (b–d) show contour of $\left(1 - B/\|\boldsymbol{\tau}\|_{\mathrm{v}}\right)_+$ at three different time sequences: (b) particle close to the plug region, (c) cutting the yield surface and entering into the plug region, (d) totally inside the plug. Please note that in panel (d), the material around the particle is yielded (light blue), while far from the particle surface, the core plug is unyielded (dark blue corresponds to zero level contour or unyielded material). (For interpretation of the references to colour in this figure legend, the reader is referred to the web version of this article.)

the particle finds its equilibrium position in the middle of the sheared region. However, by increasing the Weissenberg number to 0.5 (the red discontinuous line with △ in Fig. 2(a)), the particle migrates all the way towards the centreline by entering into the unyielded region. Here, the interesting point is that although the particle carried by the viscoelastic fluid ($B = 0$) does not migrate towards the centre of the channel or walls (indeed inertia is dominant to elastic effects), when we increase the Bingham number (i.e. in elastoviscoplastic fluid flow), the particle moves towards the centre by entering into the plug region.

Fig. 3 shows different dynamical aspects of the particle for the case $Wi = 0.5$ & $B = 0.2$. Panel (a) compares the velocity of the particle to the velocity of the undisturbed flow (see Appendix) in the streamwise direction (black lines) together with the rotation of the particle and the rotation of the fluid element in the undisturbed flow (red lines) at different wall-normal positions. As can be observed, the rotation of the particle roughly follows the vorticity of the undisturbed flow (or indeed rate of strain since the undisturbed flow is unidirectional) and vanishes gradually as it enters into the plug region and will be exactly zero at the centreline when its migration is completed. The velocity of the particle also asymptotes to the plug velocity: when the particle has reached the centreline, it translates with the plug without any relative motion/rotation. Panels (b–d) of Fig. 3 show the contour of $\left(1 - B/\|\boldsymbol{\tau}\|_{\mathrm{v}}\right)_+$ at three different instants before, during, and after particle penetration into the plug region: zero values (dark blue colour) represent the unyielded regions. It is clear that the particle yields the adjacent fluid in the unyielded plug while it is moving towards the centreline (see panel (d)).

It is worth mentioning that this interesting behaviour (i.e. entering into the plug region and moving towards the centreline) is independent of the initial position of the particle which makes it totally different from the particle-focusing in viscoelastic shear-thinning fluid flows [29]. Only two extra simulations with different initial positions ($y_p(t = 0) = -y^*$ & $y_p(t = 0) = -3.8$) are shown to avoid cluttering

Fig. 2(a), however, we have tested various starting points including the wall vicinity ($y_p(t=0) = -4.3$).

Entering the plug region is restricted to intermediate values of Wi (≈ 0.5) as by increasing the Weissenberg number to unity, the particle again finds its equilibrium position between the wall and the yield surface. This is demonstrated clearly in Fig. 2(b), where the wall-normal position of the particles are shown at $B = 0.4$ for five different Weissenberg numbers. For $Wi = 0.5$ and 0.7, the particles enter the plug region while neither for smaller nor larger Weissenberg numbers such behaviour is observed: instead, they migrate towards their stable position somewhere in the middle of the sheared region width.

For a deeper understanding of the particle migration towards the centreline by penetrating into the plug region, we shall split the whole process into two main steps: before and during/after the penetration. Firstly, let us consider the tendency of the particle to move towards the centreline while it is still in the sheared region. As mentioned above, in the viscoelastic case ($B = 0$), at $Wi = 0.5$, the particle does not end up in the centreline although the equilibrium position of the particle is closer to the centreline compared to the other Weissenberg numbers. However, at finite Bingham numbers (also at $Wi = 0.5$), it does move towards the centreline. This can be interpreted as enhanced elastic effects (which triggers particle-focusing at the centreline) in elastoviscoplastic fluid flows when Wi is fixed and the Bingham number is increased. This is in agreement with the observations made by Chaparian & Tammisola [45] for a pressure-driven flow of an elastoviscoplastic fluid in a wavy channel and by Cheddadi et al. [46] for particle sedimentation in the same type of fluids. Indeed, in the two above mentioned studies, it has been demonstrated that the asymmetry in the flow field (attributed to elastic effects) is enhanced by increasing the Bingham number at a fixed Weissenberg number. More precisely, Chaparian & Tammisola [45] quantified this asymmetry and showed that it is constant when $Wi \times B = \hat{\lambda}\,\hat{\tau}_Y/\hat{\mu}$ is constant. It might be understood considering that the stress relaxation in the case of an elastoviscoplastic fluid is not only a function of the viscosity, but also the yield stress would play a role in dissipation. Hence, the *effective* Weissenberg number in an elastoviscoplastic fluid increases with the Bingham number.

Now let us consider the second step. In the following, we explain how the particle inertia and rotation enables particle penetration and migration inside the plug region. It is clear from Fig. 3(a) that the particle rotation is non-zero when the particle touches the plug region. The particle rotation (and to a lesser extent translation) increases the shear around it; the particle yields the adjacent material and enters into the plug region. Fig. 4 illustrates the axial velocity profile during the particle penetration (the blue line). It clearly shows how the fluid velocity changes with respect to the undisturbed flow: indeed the flow field adjusts itself so that the difference between the velocity gradients on the two sides of the particle (top and bottom) is decreased compared to the undisturbed flow. This markedly reduces the only negative force contribution—shear-gradient force towards the wall [47]—and facilitates the particle penetration. On the other hand, once the particle has fully entered into the plug region, the velocity of the material surrounding it is roughly constant (i.e. equal to the plug velocity) except in the narrow region which is yielded around the particle. The particle also rotates clockwise, hence, there is a lift acting on the particle which pushes it towards the centreline—Magnus lift force (see Fig. 1(a) of [48]). Simultaneously, there is a non-zero first normal stress difference (N_1) due to the material elasticity acting over the particle surface which also pushes it towards the centreline.

The particle migration to the centreline is hence possible for those particles that start outside the plug and therefore have non-zero rotation when they hit the plug. This should not be confused with the particles initially fully immersed in the plug; those particles translate with the plug without any rotation/migration as mentioned earlier. Indeed, both the first mechanism (rotating and yielding the adjacent material) and the Magnus lift force are absent in those cases. It is worth

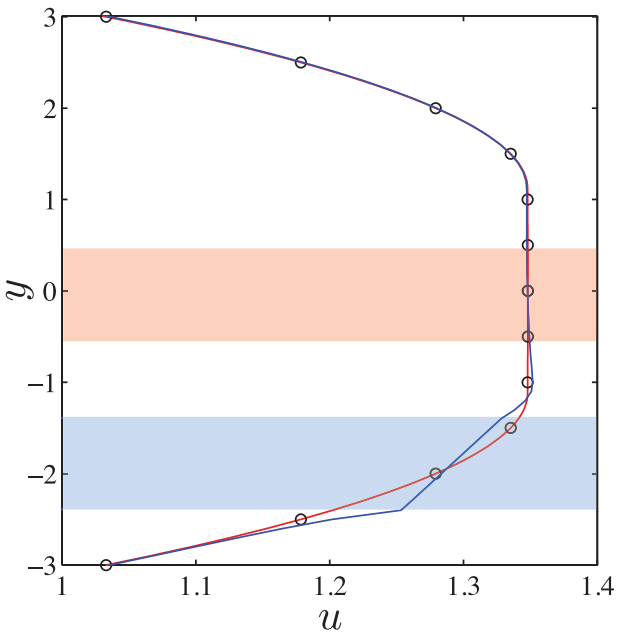

Fig. 4. Axial velocity profiles for the case $Wi = 0.5$ & $B = 0.2$ at the particle centre position (x_p): black circles represent the undisturbed flow (Appendix), blue line corresponds to a time just before the particle penetration (when the top surface of the particle is very close to y^*; the same as the panel (b) of Fig. 3) and red line at the moment when the migration is completed. Blue and red shadows mark inside the particles with the same colour interpretation. (For interpretation of the references to colour in this figure legend, the reader is referred to the web version of this article.)

mentioning that particles entering the plug region slowly migrate all the way towards the centreline where N_1 and the shear stress go to zero (see Appendix), although they do so over a longer time compared to the migration in the sheared regions since the effective viscosity is high in the plug region and also particle rotation decays gradually as the particle approaches the centreline which results in smaller Magnus lift force.

Another interesting feature to investigate is the distance between the stable position of the particle and the yield surface as a function of the Bingham number; see Fig. 5. In the range of Weissenberg numbers studied, the position of the yield surface does not change considerably with Wi, hence, we use the value of y^* at the limit $Wi \to 0$ in this figure (see Appendix). It can be observed that $y^e - y^*$ does not change remarkably (≈ 2) at the smallest Weissenberg number (i.e. $Wi = 0.1$: square symbols in Fig. 5). This observation implies that at this small Weissenberg number (associated with the viscoplastic limit), by increasing the Bingham number, the core unyielded plug will grow thicker and consequently the particle stable position will be pushed towards the wall by roughly the same amount. In other words, in the viscoplastic limit, particles feel a smaller channel width since the part of the flow close to the centreline moves as a plug with constant velocity and $\dot{\gamma} = 0$. However, in the elastoviscoplastic regime (larger Weissenberg numbers), namely $Wi = 1$ (asterisk symbols), $y^e - y^*$ deviates considerably from a plateau due to high elastic effects. For the moderate Weissenberg numbers (e.g. $Wi = 0.5$) and non-zero Bingham numbers, as shown above particles enter into the plug region and move towards the centreline, which corresponds to the negative values in Fig. 5.

4. Final remarks

In the present study, we investigated the migration of neutrally buoyant spherical particles within the channel Poiseuille flow of an elastoviscoplastic fluid by three-dimensional direct numerical simulations.

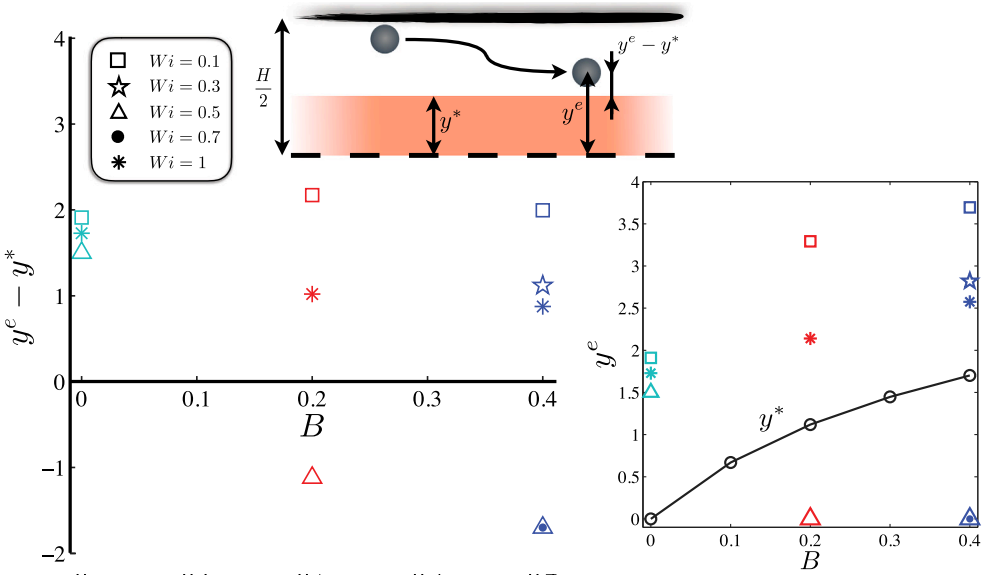

Fig. 5. Distance between the final position of the particles (y^e) and the yield surface versus the Bingham number. The symbols and colours interpretation are the same as Fig. 2. The position of the yield surface (y^*) for $Wi \to 0$ is used. Please note that in the range of Weissenberg numbers studied, the position of the yield surface does not change considerably. The inset shows y^e and y^* individually versus B.

For the range of studied parameters ($\xi = 10, Re = 20, 0.1 \leqslant Wi \leqslant 1, 0 \leqslant B \leqslant 0.4$), in the viscoelastic limit, inertia is dominant and particles find their equilibrium position between the centreline and the walls. In the viscoplastic limit, the behaviour is the same, although the yield surface takes the role of the centreline and particles only migrate in the sheared regions. In this limit, the particle equilibrium position shifts towards the wall by increasing the Bingham number since the plug region grows: the distance between the particle final position and the plug surface remains approximately constant.

In the intermediate regime in which the suspending fluid exhibits both elastic and plastic behaviours, we demonstrated that particle focusing at the centreline can be achieved: particles can enter the plug region and migrate towards the centreline for a specific range of Weissenberg numbers in an elastoviscoplastic fluid. This is attributed to the particle rotation that partially yields the plug region and then the combination of the elastic forces and Magnus lift force push the particle towards the centre where all the forces go to zero.

This phenomenon could be directly used in particle sorting or cell manipulation in the inertial regime, which is nearly impossible in viscoelastic fluids. As reported by li et al. [29], particle focusing in viscoelastic fluids happens at elastic numbers (Wi/Re) beyond $O(1)$ (in the present scalings; we used $\hat{D}$ as the length scale). However, here we have shown that elastoviscoplastic fluids are capable to reduce the desirable elastic number for particle focusing to $O(10^{-2})$. More interestingly, here the particle-focusing at the centreline is independent of the particle initial position, in contrast to the migration inside the viscoelastic shear-thinning fluids [25,29]. Please note that the viscoelastic part of the used rheological model – Saramito model – is based on the Oldroyd-B model which is not shear-thinning.

As we mentioned in Section 2, in defining the Reynolds number and the other non-dimensional numbers, one can use the effective viscosity, for instance, the *effective* Reynolds number, $Re_{eff} = Re/(1 + B)$, which is tremendously helpful in analysing the internal flows of yield-stress fluids [35,49]. However, due to the limited range of studied parameters in the present problem, we continued with the classical definitions to make any further comparison easier: the smallest effective Reynolds number ($B = 0.4$) is approximately 14.29 which is still large. It is clearly evidenced in the simulation $Wi = 0.1$ & $B = 0.4$ (blue squares-continuous line in Fig. 2) in which the particle migrates a lot in the absence of significant elastic effects. Moreover, an *effective* Weissenberg number could be useful which increases with the Bingham number as discussed in Section 3. We shall postpone this to future studies with a larger range of studied parameters.

A lot still remains to be understood about the transport of suspensions in yield-stress fluids. Although computational studies of these problems are extremely expensive, here we shed light on a range of important parameters and some exceptional behaviours of the particle dynamics. The present study provides some base fundamental results from which to look at more detailed studies in the entire parametric space and more complex cases.

Declaration of competing interest

The authors declare that they have no known competing financial interests or personal relationships that could have appeared to influence the work reported in this paper.

Acknowledgements

E.C. gratefully acknowledges the Linné FLOW PostDoc grant during the course of this study. E.C. and O.T. appreciate the support of Swedish Research Council through grant VR 2017–0489. L.B. appreciates the support of Swedish Research Council through grant VR 2014–5001. The computational time provided by SNIC (Swedish National Infrastructure for Computing) is highly acknowledged. We thank the referees for their constructive comments which helped us a lot in improving the physical discussion in this paper.

Appendix. Exact solution of the background flow

Here we derive the exact solution for the single-phase elastoviscoplastic fluid channel flow. For a fully-developed parallel flow, the governing equations reduce to,

$$\frac{\mathrm{d}\tau_{xy}}{\mathrm{d}y} + \beta\frac{\mathrm{d}^2u}{\mathrm{d}y^2} = Re\frac{\mathrm{d}p}{\mathrm{d}x} = -Re\ G, \tag{A.1a}$$

$$\frac{\mathrm{d}\tau_{yy}}{\mathrm{d}y} = 0, \tag{A.1b}$$

and the fluid behaviour obeys,

$$-2\ Wi\ \tau_{xy}\frac{\mathrm{d}u}{\mathrm{d}y} + \left(1 - \frac{B}{\|\boldsymbol{\tau}\|_{\mathrm{v}}}\right)_{+}\tau_{xx} = 0, \tag{A.2a}$$

$$-Wi\ \tau_{yy}\frac{\mathrm{d}u}{\mathrm{d}y}+\left(1-\frac{B}{\|\boldsymbol{\tau}\|_{\mathrm{v}}}\right)_{+}\tau_{xy}=(1-\beta)\frac{\mathrm{d}u}{\mathrm{d}y}, \tag{A.2b}$$

$$\left(1-\frac{B}{\|\boldsymbol{\tau}\|_{\mathrm{v}}}\right)_{+}\tau_{yy}=0. \tag{A.2c}$$

Expression (A.2c) clearly shows that in the sheared regions $\tau_{yy}=0$. Hence from Eq. (A.1b) we deduce that in the whole gap $\tau_{yy}=0$. Integrating Eq. (A.1a) yields an expression for τ_{xy},

$$\tau_{xy}=-Re\ G\ y-\beta\ \frac{\mathrm{d}u}{\mathrm{d}y} \tag{A.3}$$

or alternatively, $\dfrac{\mathrm{d}u}{\mathrm{d}y}=-\dfrac{Re\ G\ y+\tau_{xy}}{\beta}$.

Given that $\tau_{yy}=0$ and in the yielded regions $\dfrac{\mathrm{d}u}{\mathrm{d}y}\neq 0$, from expressions (A.2a), (A.2b), one can conclude that $\tau_{xx}=\dfrac{2\ Wi\ \tau_{xy}^2}{1-\beta}$, or, $\|\boldsymbol{\tau}\|_{\mathrm{v}}=\sqrt{\tau_{xy}^2+\dfrac{Wi^2\ \tau_{xy}^4}{(1-\beta)^2}}$, which suggests that τ_{xy} should satisfy,

$$\left(1-\frac{B}{\|\boldsymbol{\tau}\|_{\mathrm{v}}}\right)\tau_{xy}=\frac{\beta-1}{\beta}(Re\ G\ y+\tau_{xy}), \tag{A.4}$$

in the yielded regions. By using a simple zero-finding method, expression (A.4) gives the shear stress in the whole channel width provided that the proper G is used. From the continuity equation we know that $\xi=2\int_0^{\xi/2}u\ \mathrm{d}y$ which can be converted to,

$$\xi=\frac{Re\ G\ \xi^3}{12\beta}+\frac{2}{\beta}\int_0^{\xi/2}y\ \tau_{xy}\ \mathrm{d}y, \tag{A.5}$$

using integration by parts. Hence, G and τ_{xy} can be found in a trial-and-error procedure using (A.4) and (A.5). Then simple numerical integration of Eq. (A.3) gives the velocity profile in the channel. It is worth mentioning that the position of the yield surface can be found as,

$$y^*=\pm\left(\frac{\sqrt{1+\frac{4\ Wi^2\ B^2}{(1-\beta)^2}}-1}{2\frac{Wi^2\ Re^2\ G^2}{(1-\beta)^2}}\right)^{\frac{1}{2}} \tag{A.6}$$

which reduces to $\pm\frac{B}{Re\ G}$ in the viscoplastic limit $Wi\to 0$ [50]. Please note that in the core unyielded region, τ_{xx} is mathematically undetermined; the only restriction is $|\tau_{xx}|\leqslant 2\sqrt{B^2-Re^2G^2y^2}$. If $\beta=0$ (neo-Hookean solid behaviour before yielding), then a closed-form solution to the flow can be derived; see [45].

References

[1] M.S. Choi, Y.J. Kim, S.H. Kwon, Prediction on pipe flow of pumped concrete based on shear-induced particle migration, Cem. Concr. Res. 52 (2013) 216–224.
[2] S. Hormozi, I.A. Frigaard, Dispersion of solids in fracturing flows of yield stress fluids, J. Fluid Mech. 830 (2017) 93–137.
[3] G. Segré, A. Silberberg, Radial particle displacements in Poiseuille flow of suspensions, Nature 189 (4760) (1961) 209.
[4] G. Segré, A.G. Silberberg, Behaviour of macroscopic rigid spheres in Poiseuille flow part 2. Experimental results and interpretation, J. Fluid Mech. 14 (1) (1962) 136–157.
[5] G. Segré, A.J. Silberberg, Behaviour of macroscopic rigid spheres in Poiseuille flow part 1. Determination of local concentration by statistical analysis of particle passages through crossed light beams, J. Fluid Mech. 14 (1) (1962) 115–135.
[6] B.P. Ho, L.G. Leal, Inertial migration of rigid spheres in two-dimensional unidirectional flows, J. Fluid Mech. 65 (2) (1974) 365–400.
[7] J.A. Schonberg, E.J. Hinch, Inertial migration of a sphere in Poiseuille flow, J. Fluid Mech. 203 (1989) 517–524.
[8] A.J. Hogg, The inertial migration of non-neutrally buoyant spherical particles in two-dimensional shear flows, J. Fluid Mech. 272 (1994) 285–318.
[9] J.-P. Matas, J.F. Morris, E. Guazzelli, Inertial migration of rigid spherical particles in poiseuille flow, J. Fluid Mech. 515 (2004) 171–195.
[10] I. Lashgari, M.N. Ardekani, I. Banerjee, A. Russom, L. Brandt, Inertial migration of spherical and oblate particles in straight ducts, J. Fluid Mech. 819 (2017) 540–561.
[11] A. Kilimnik, W. Mao, A. Alexeev, Inertial migration of deformable capsules in channel flow, Phys. Fluids 23 (12) (2011) 123302.
[12] S.C. Hur, S.-E. Choi, S. Kwon, D. Di Carlo, Inertial focusing of non-spherical microparticles, Appl. Phys. Lett. 99 (4) (2011) 044101.
[13] D. Alghalibi, M.E. Rosti, L. Brandt, Inertial migration of a deformable particle in pipe flow, Phys. Rev. Fluids 4 (10) (2019) 104201.
[14] O. Merkak, L. Jossic, A. Magnin, Dynamics of particles suspended in a yield stress fluid flowing in a pipe, AIChE J. 54 (5) (2008) 1129–1138.
[15] O. Merkak, L. Jossic, A. Magnin, Migration and sedimentation of spherical particles in a yield stress fluid flowing in a horizontal cylindrical pipe, AIChE J. 55 (10) (2009) 2515–2525.
[16] E. Chaparian, O. Tammisola, Stability of particles inside yield-stress fluid Poiseuille flows, J. Fluid Mech. 885 (2020) A45.
[17] D. Yuan, Q. Zhao, S. Yan, S.Y. Tang, G. Alici, J. Zhang, W. Li, Recent progress of particle migration in viscoelastic fluids, Lab Chip 18 (4) (2018) 551–567.
[18] D.M. Martinez, J.A. Olson, A. Madani, I.A. Frigaard, D. Farajisarir, J. Lockhart, Method and apparatus for continuously fractionating particles contained within a viscoplastic fluid, 2017, uS Patent 9849466 (Dec. 26 2017).
[19] D. Feys, G. De Schutter, R. Verhoeven, Parameters influencing pressure during pumping of self-compacting concrete, Mater. Struct. 46 (4) (2013) 533–555.
[20] D. Kaplan, F. De Larrard, T. Sedran, Avoidance of blockages in concrete pumping process, ACI Mater. J. 102 (3) (2005) 183.
[21] P. Saramito, A new constitutive equation for elastoviscoplastic fluid flows, J. Non-Newton. Fluid Mech. 145 (1) (2007) 1–14.
[22] F.P. Bretherton, The motion of rigid particles in a shear flow at low Reynolds number, J. Fluid Mech. 14 (2) (1962) 284–304.
[23] A. Karnis, S.G. Mason, Particle motions in sheared suspensions. xix. Viscoelastic media, Trans. Soc. Rheol. 10 (2) (1966) 571–592.
[24] F. Gauthier, H.L. Goldsmith, S.G. Mason, Particle motions in non-Newtonian media. ii. Poiseuille flow, Trans. Soc. Rheol. 15 (2) (1971) 297–330.
[25] M.M. Villone, G. D'avino, M.A. Hulsen, F. Greco, P.L. Maffettone, Numerical simulations of particle migration in a viscoelastic fluid subjected to Poiseuille flow, Comput. Fluids 42 (1) (2011) 82–91.
[26] D. Di Carlo, J.F. Edd, K.J. Humphry, H.A. Stone, M. Toner, Particle segregation and dynamics in confined flows, Phys. Rev. Lett. 102 (9) (2009) 094503.
[27] A.H. Raffiee, A.M. Ardekani, S. Dabiri, Numerical investigation of elasto-inertial particle focusing patterns in viscoelastic microfluidic devices, J. Non-Newton. Fluid Mech. 272 (2019) 104166.
[28] M. Trofa, M. Vocciante, G. D'Avino, M.A. Hulsen, F. Greco, P.L. Maffettone, Numerical simulations of the competition between the effects of inertia and viscoelasticity on particle migration in Poiseuille flow, Comput. Fluids 107 (2015) 214–223.
[29] G. Li, G.H. McKinley, A.M. Ardekani, Dynamics of particle migration in channel flow of viscoelastic fluids, J. Fluid Mech. 785 (2015) 486–505.
[30] I.R. Siqueira, P.R. de Souza Mendes, On the pressure-driven flow of suspensions: particle migration in apparent yield-stress fluids, J. Non-Newton. Fluid Mech. 265 (2019) 92–98.
[31] E. Chaparian, I.A. Frigaard, Cloaking: Particles in a yield-stress fluid, J. Non-Newton. Fluid Mech. 243 (2017) 47–55.
[32] E. Chaparian, I.A. Frigaard, Yield limit analysis of particle motion in a yield-stress fluid, J. Fluid Mech. 819 (2017) 311–351.
[33] E. Chaparian, A. Wachs, I.A. Frigaard, Inline motion and hydrodynamic interaction of 2D particles in a viscoplastic fluid, Phys. Fluids 30 (3) (2018) 033101.
[34] C.J. Dimitriou, G.H. McKinley, A comprehensive constitutive law for waxy crude oil: a thixotropic yield stress fluid, Soft Matter 10 (35) (2014) 6619–6644.
[35] R.L. Thompson, E.J. Soares, Viscoplastic dimensionless numbers, J. Non-Newton. Fluid Mech. 238 (2016) 57–64.
[36] D. Izbassarov, M.E. Rosti, M.N. Ardekani, M. Sarabian, S. Hormozi, L. Brandt, O. Tammisola, Computational modeling of multiphase viscoelastic and elastoviscoplastic flows, Internat. J. Numer. Methods Fluids 88 (12) (2018) 521–543.
[37] M.E. Rosti, D. Izbassarov, O. Tammisola, S. Hormozi, L. Brandt, Turbulent channel flow of an elastoviscoplastic fluid, J. Fluid Mech. 853 (2018) 488–514.
[38] E. Chaparian, D. Izbassarov, F. De Vita, L. Brandt, O. Tammisola, Yield-stress fluids in porous media: a comparison of viscoplastic and elastoviscoplastic flows, Meccanica 55 (2020) 331–342.
[39] W.-P. Breugem, A second-order accurate immersed boundary method for fully resolved simulations of particle-laden flows, J. Comput. Phys. 231 (13) (2012) 4469–4498.
[40] M.A. Hulsen, R. Fattal, R. Kupferman, Flow of viscoelastic fluids past a cylinder at high Weissenberg number: stabilized simulations using matrix logarithms, J. Non-Newton. Fluid Mech. 127 (1) (2005) 27–39.
[41] R. Fattal, R. Kupferman, Time-dependent simulation of viscoelastic flows at high Weissenberg number using the log-conformation representation, J. Non-Newton. Fluid Mech. 126 (1) (2005) 23–37.
[42] R. Keunings, On the high Weissenberg number problem, J. Non-Newton. Fluid Mech. 20 (1986) 209–226.
[43] C.-W. Shu, High order weighted essentially nonoscillatory schemes for convection dominated problems, SIAM 51 (1) (2009) 82–126.

[44] M.N. Ardekani, P. Costa, W.P. Breugem, L. Brandt, Numerical study of the sedimentation of spheroidal particles, Int. J. Multiph. Flow 87 (2016) 16–34.
[45] E. Chaparian, O. Tammisola, An adaptive finite element method for elastoviscoplastic fluid flows, J. Non-Newton. Fluid Mech. (2019) 104148.
[46] I. Cheddadi, P. Saramito, B. Dollet, C. Raufaste, F. Graner, Understanding and predicting viscous, elastic, plastic flows, Eur. Phys. J. E 34 (1) (2011) 1.
[47] J.M. Martel, M. Toner, Inertial focusing in microfluidics, Annu. Rev. Biomed. Eng. 16 (2014) 371–396.
[48] J. Zhang, S. Yan, D. Yuan, G. Alici, N.-T. Nguyen, M.E. Warkiani, W. Li, Fundamentals and applications of inertial microfluidics: a review, Lab Chip 16 (1) (2016) 10–34.
[49] A.B. Metzner, J.C. Reed, Flow of non-Newtonian fluids—correlation of the laminar, transition, and turbulent-flow regions, AIChE J. 1 (4) (1955) 434–440.
[50] I.A. Frigaard, C. Nouar, On the usage of viscosity regularisation methods for visco-plastic fluid flow computation, J. Non-Newton. Fluid Mech. 127 (1) (2005) 1–26.